https://doi.org/10.5194/tc-2019-168
Preprint. Discussion started: 10 September 2019

The Cryosphere Discussions

Incorporating moisture content in surface energy balance modeling of a debris-covered glacier

Alexandra Giese[1], Aaron Boone[2], Patrick Wagnon[3], and Robert Hawley[1]

[1]Department of Earth Sciences, Dartmouth College, Hanover NH USA
[2]CNRM-GAME - Groupe d'Étude de l'Atmosphère Météorologique, Toulouse FRANCE
[3]Univ. Grenoble Alpes, CNRS, IRD, Grenoble-INP, IGE, 38000 Grenoble FRANCE

Correspondence: Alexandra Giese (algiese@gmail.com)

Abstract. Few surface energy balance models for debris-covered glaciers account for the presence of moisture in the debris, which invariably affects the debris layer's thermal properties and, in turn, the surface energy balance and sub-debris melt of a debris-covered glacier. We adapted the Interactions between Soil, Biosphere, and Atmosphere (ISBA) land surface model within the SURFace EXternalisée (SURFEX) platform to represent glacier debris rather than soil. The new ISBA-DEBris model includes the varying content, transport, and state of moisture in debris with depth and through time. It robustly simulates not only the thermal evolution of the glacier-debris-snow column but also moisture transport and phase changes within the debris – and how these, in turn, affect conductive and latent heat fluxes. We discuss the key developments in the adapted ISBA-DEB and demonstrate the capabilities of the model, including how the time- and depth-varying thermal conductivity and specific heat capacity depend on evolving temperature and moisture. Sensitivity tests emphasize the importance of accurately constraining the roughness lengths and surface slope. Emissivity, in comparison to other tested parameters, has less of an effect on melt. ISBA-DEB builds on existing work to represent the energy balance of a supraglacial debris layer through time in its novel application of a land surface model to debris covered glaciers. Comparison of measured and simulated debris temperatures suggests that ISBA-DEB includes some – but not all – processes relevant to melt under highly permeable debris. Future work, informed by further observations, should explore the importance of advection and vapor transfer.

1 Introduction

Enhancing the melt of underlying ice when thin and inhibiting it when thick (Östrem, 1959), supraglacial debris is known to affect the surface energy balance and retreat patterns of mountain glaciers. Supraglacial debris covers 11% of glacier area in High Mountain Asia (HMA) (Kraaijenbrink et al., 2017), a region that contains the highest volume of ice on Earth outside the polar regions and where glacier melt flows into rivers that deliver water to 800 million people (Pritchard, 2019). Understanding sub-debris melt is crucial for making informed projections of climate change impacts and associated water security issues in HMA.

Sub-debris ablation is fundamentally a function of the temperature at the surface of the debris and the ability of the debris to conduct heat to its base at the ice-debris interface. Therefore, the amount of ice melt under debris is determined by local

https://doi.org/10.5194/tc-2019-168
Preprint. Discussion started: 10 September 2019

The Cryosphere Discussions

meteorological conditions and physical properties of the debris itself. Debris properties beyond thickness are inherently difficult to constrain; a debris layer is filled with rock clasts of different sizes, angularities, and lithologies that are distributed and sorted heterogeneously over the ablation zone. A debris layer's interstitial spaces may be comprised of air or percolating water, which itself undergoes phase changes as a function of temperature.

Moisture has been largely unaddressed in glacier models, despite the fact that water and ice affect the thermal properties of a debris layer and the efficiency with which heat is conducted through debris. Table 1 contrasts bulk thermal conductivity, heat capacity, and density of dry debris (porosity ϕ = 0.39) with debris of the same porosity that has water-filled and ice-filled interstitial spaces. A number of studies (e.g. Conway and Rasmussen, 2000; Reznichenko et al., 2010; Nicholson and Benn, 2012; Collier et al., 2014) have emphasized the importance of moisture to the thermal properties of debris, particularly in transition seasons. Rounce and McKinney (2014) found a dramatic increase in conductivity from the top 10 cm of debris on Khumbu region glaciers to the deeper depths; they attribute this difference to water content, noting that Nicholson and Benn (2006) found the conductivity of fully saturated debris to be a factor of 2–3 greater than that of dry. Importantly, water content shows an association with grain size, too: coarser sediments are less likely to have wet surfaces because fine-grained sediment has small void spaces and, thus, greater capacity for water retention (Juen et al., 2013; Blum et al., 2018).

Further, evaporation and sublimation will lower the surface temperature and remove mass from the system. Condensation and deposition have the opposite effect. Sakai et al. (2004) suggest that neglecting evaporation in energy balance computations can cause an overestimation of sub-debris melt rates by a factor of two.

Most existing models have assumed a dry debris layer, with rain, snowmelt, and glacier melt running off instantaneously (e.g. Reid and Brock, 2010; Lejeune et al., 2013; Rounce and McKinney, 2014). The few studies that do address moisture focus on end member cases (Nakawo and Young, 1981; Nicholson and Benn, 2006), account for moisture only when relative humidity is 100% (Reid and Brock, 2010; Reid et al., 2012; Fyffe et al., 2014), incorporate a thickness-dependent "wetness factor" (Fujita and Sakai, 2014), or parameterize latent heat based on relative humidity and rain (Rounce et al., 2015).

Collier et al. (2014) introduced the first energy-balance model that included an evolving, partially saturated debris layer. The model treated moisture through a reservoir approach and calculated the water vapor partial pressure gradient to inform calculations of latent heat fluxes within the debris. This study laid the groundwork for modeling moisture and identified the need for a physically-based approach to incorporating vertical transport processes (i.e. capillary action, hydraulic gradient-driven flow, etc.) and to prognosing the distribution and phase changes of moisture with depth and through time.

Here, we introduce a model that, to our knowledge, is the first to incorporate moisture with consideration of its vertical transport processes and distribution in debris; ISBA-DEB is capable of representing vertical moisture fluxes, phase changes, and moisture retention. We adapt the Interactions between Soil, Atmosphere, and Biosphere (ISBA) soil model housed within the SURFace EXternalisée (SURFEX) platform of Météo-France to include boundary conditions, thermal properties, hydraulic properties, and runoff parameterizations appropriate for supraglacial debris. The ISBA-DEB model is capable of solving not only the heat equation but also moisture transport and retention via the mixed-form Richards' equation.

https://doi.org/10.5194/tc-2019-168
Preprint. Discussion started: 10 September 2019

The Cryosphere Discussions
Open Access
EGU

Debris porosity (ϕ) = 0.39	**Conductivity ($\mathbf{W\,m^{-1}K^{-1}}$)**	**Heat capacity ($\mathbf{J\,kg^{-1}K^{-1}}$)**	**Density ($\mathbf{kg\,m^{-3}}$)**	**Volumetric Heat capacity ($\mathbf{J\,m^{-3}K^{-1}}$)**	**Diffusivity ($\mathbf{m^2\,s^{-1}}$)**
Dry debris	**0.94 (Reid and Brock, 2010)**	**948 (Brock et al., 2010)**	**1690**	**948*1690=1602120**	**5.867 $\times 10^-7$**
Air	0.024	1000	$P/(R_d * T_v)$	-	-
Water-saturated debris	**0.94+0.39*0.57=1.16**	**-**	**-**	**948*1690+0.39*4218*1000=3247140**	**3.572 $\times 10^-7$**
Water	0.57	4218	1000	-	-
Ice-saturated debris	**0.94+0.39*2.22=1.81**	**-**	**-**	**948*1690+0.39*2110*917=2356700**	**7.680 $\times 10^-7$**
Ice	2.2	2110	917	-	-

Table 1. Thermally relevant properties of dry debris, in which interstitial pore spaces are filled with air; water-saturated debris; and ice-saturated debris of porosity (ϕ) = 0.39. Air density is a function of elevation, air temperature, and air moisture. In the equation for air density, $\rho_{air} = P/(R_d * T_v)$, P is pressure (Pa), R_d is the gas constant for dry air ($\sim$ 287 J kg^{-1}K^{-1}), and T_v is the virtual temperature (K). Thermal conductivity presented by Reid and Brock (2010) is an "effective" value, from measurements, that is a function of debris' unspecified porosity and any moisture content at the time of measurement (Collier et al., 2016). Brock et al. (2010) used a published value of specific heat (948 J kg^{-1}K^{-1}). We assume that these values of thermal conductivity and heat capacity listed for dry debris are valid for dry debris on West Changri Nup glacier and subsequently perform sensitivity tests. Note that diffusivity is conductivity normalized by volumetric heat capacity.

https://doi.org/10.5194/tc-2019-168
Preprint. Discussion started: 10 September 2019

The Cryosphere Discussions
Open Access

In this paper, we show capabilities of the model, evaluate its performance, and conduct a series of sensitivity tests on input parameters. We ran ISBA-DEB by driving it with two years of gap-filled *in situ* meteorological data from West Changri Nup glacier and compared output to debris measurements over the same period.

We highlight the important physical processes that need to be accounted for in any debris covered glacier melt model, such as conduction and phase change of water and ice in the debris. We also discuss the limitations of our model and propose some further considerations for making improvements.

2 Field Site: West Changri Nup Glacier

West Changri Nup glacier (Figure 1, 27.97 ^{o}N, 86.76 ^{o}E), also known as White Changri Nup glacier, has an area of 0.92 km^2, ranges in elevation 5330 – 5690 m, and has a small debris covered area despite being mostly clean. It lies 200 m southeast of North Changri Nup glacier (Sherpa et al., 2017; Vincent et al., 2016) in the Mt. Everest region of Nepal. The ablation zone of North Changri Nup glacier is dominated by a debris cover that has an insulating effect on mass balance (Vincent et al., 2016). Ice cliffs, despite imparting a localized ablation rate of ∼3 times that of the glacier tongue, do not compensate for the ablation reduction impact of the debris on North Changri Nup glacier (Brun et al., 2018). Field measurements and observations confirm the presence of water in debris: density measurements at four sites show that deeper debris retains more moisture, and water has been observed to both wet the debris and pool within it.

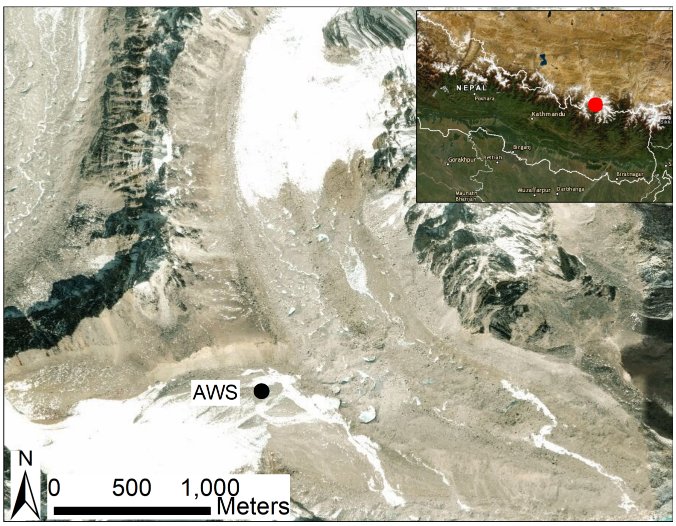

Figure 1. A map of West Changri Nup and North Changri Nup glaciers, showing the location of the AWS described in Section 4.1, with an inset map of Nepal. Source: Esri, DigitalGlobe, GeoEye, Earthstar Geographics, CNES/Airbus DS, USDA, USGS, AeroGRID, IGN, and the GIS User Community.

https://doi.org/10.5194/tc-2019-168
Preprint. Discussion started: 10 September 2019

3 ISBA-DEB

3.1 Model Overview

The ISBA land surface model (Noilhan and Planton, 1989) within the SURFEX community-based open source software platform maintained by Météo-France (Masson et al., 2013) is a physically based scheme that solves both time- and depth-dependent heat and moisture diffusion numerically through mass- and heat-conserving implicit time schemes. It provides a convenient basis for simulating the surface energy balance of a supraglacial debris layer, after making modifications to account for the differences between soil and debris. This work builds on that of Lejeune et al (2013), which used one of the SURFEX snow models, Crocus, to represent dry debris year-round, accounting for snowfall and sub-freezing glacier temperatures during the accumulation season. However, we instead adapted the diffusive version of SURFEX's soil model (ISBA option DIF). As the full details of the ISBA-DIF option for heat and moisture transfer and water phase changes within soil are presented in a series of publications (Boone et al., 1999, 2000; Decharme et al., 2011, 2013), they will be only summarized here to provide context for the detailed modifications in the supraglacial debris model, ISBA-DEB. By adapting ISBA, we have built a model that not only simulates a supraglacial debris layer's temperature and moisture but also computes glacier melt.

3.2 Model Structure

ISBA-DEB computes temperature and moisture in a snow-debris-ice column. Temperature and moisture evolution are calculated for 10–15 debris layers with user-specified thicknesses. Debris layers are assigned thermal, hydraulic, and physical properties of glacial debris as informed by field measurements on West Changri Nup glacier or, when unknown, by the debris-covered glacier literature. The underlying layers (up to 20 total layers are permitted by the model) approximate a glacier. In ISBA, the glacier layers must be soil, but in ISBA-DEB we assigned them a porosity of 99.9% and specified that they be ice-saturated. Since 99.9% of the volume of these layers is filled with solid ice, glacier layers have an effective porosity of zero.

Glacier melt enters the debris at the base, and rain and snowmelt enter the debris at the surface. Precipitation, wind, air temperature and humidity, and surface fluxes measured on West Changri Nup glacier drive the model. A discussion of the forcing variables can be found in Section 4. Figure 2 schematically shows the configuration of the domain and summarizes fluxes and processes in the 1-dimensional ISBA-DEB.

https://doi.org/10.5194/tc-2019-168
Preprint. Discussion started: 10 September 2019

The Cryosphere Discussions
Open Access
EGU

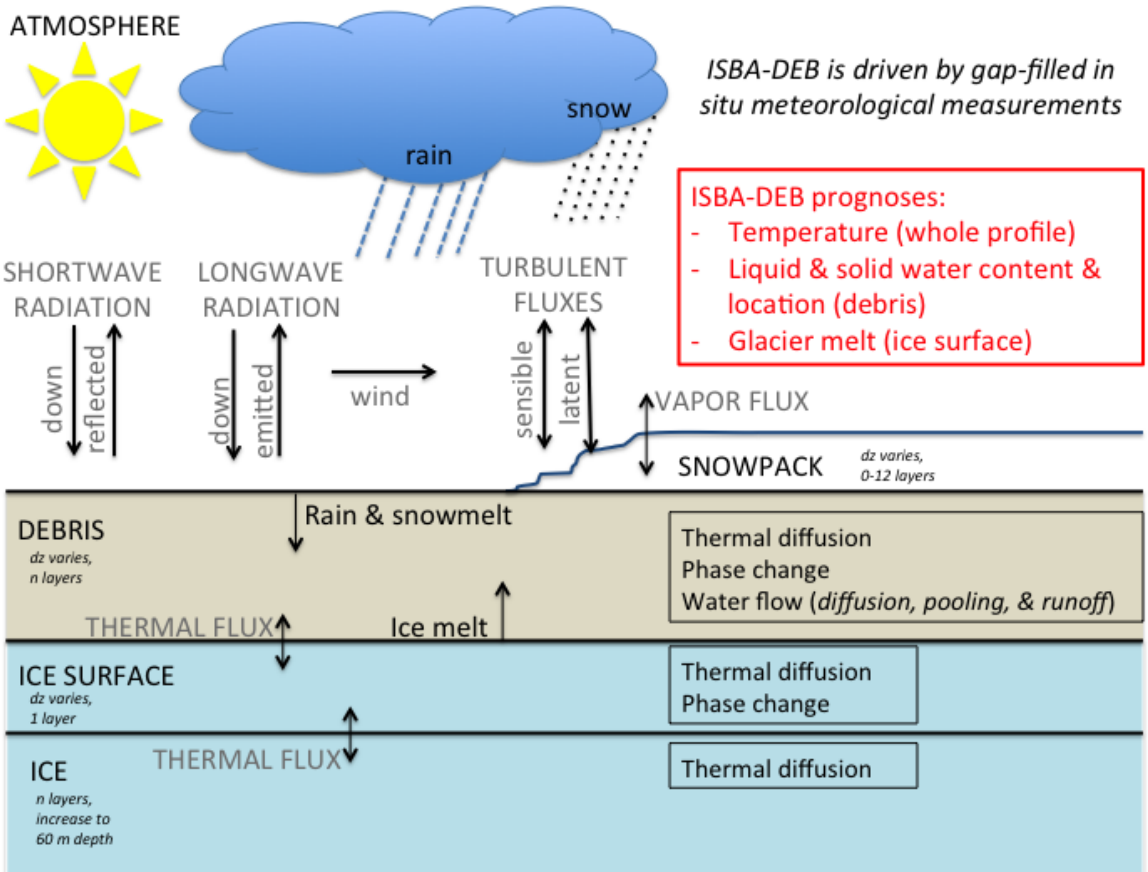

Figure 2. General scheme of ISBA-DEB, with fluxes and physical processes. Note that ISBA-DEB is a point-scale model but that the schematic is shown in 2D for interpretability. The snow scheme used in ISBA-DEB is ISBA-ES (Boone and Etchevers, 2001; Decharme et al., 2016).

ISBA-DEB, like ISBA, solves the temperature in all layers of the domain; the temperature profile is then passed to a routine that computes energy fluxes, including evaporation and glacier melt. The volume of glacier melt and the temperature profile, which has been updated with any melt that occurred during the timestep, pass into the hydrology routines that calculate water volume and location in all allowed layers – as well as its phase according to temperature (Wagnon et al., 2009). Given that the measured debris thickness of 12.5 cm is accurate to ±1 cm, we use 13 1 cm layers of debris in ISBA-DEB. The prognostic state variables are assumed to be located at the midpoint of each layer. Under the 13 debris layers are 7 layers of ice, with increasing thicknesses. The layer boundaries in the glacier are at 0.16, 0.45, 2.25, 7.00, 20.0, and 30.0 m in depth. The model reaches steady state after 40 years of spin up, given an initial uniform temperature of 268.35 K and an initial uniform liquid soil water index of 0.1 m^3 m^{-3}; other initial conditions require a longer spin up.

https://doi.org/10.5194/tc-2019-168
Preprint. Discussion started: 10 September 2019

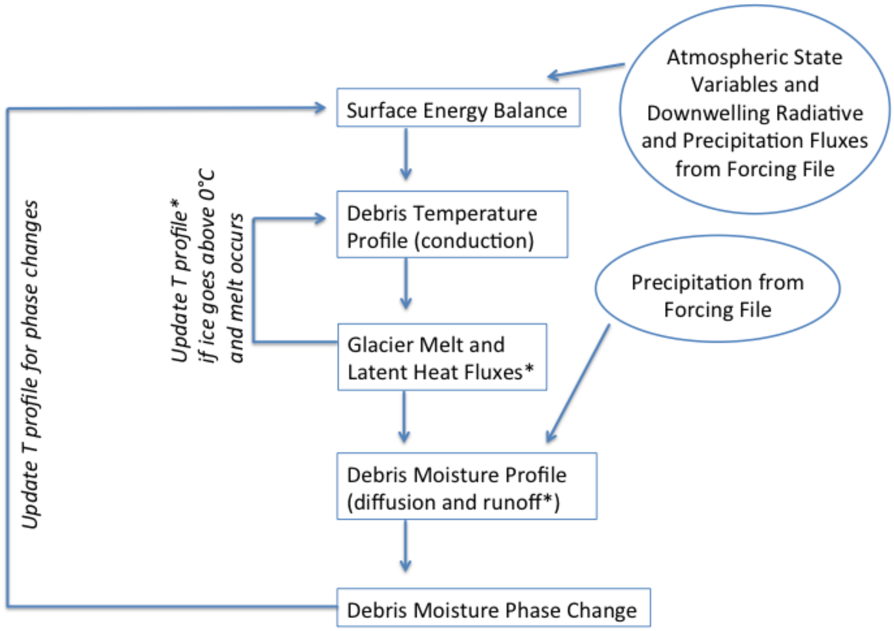

Figure 3. Flow of the processes in the ISBA-DEB model. The asterisks indicate major changes introduced to the ISBA code in the creation of ISBA-DEB. Table A1 contains physical constants and model parameters used for the runs on West Changri Nup glacier.

3.3 Physical Processes

3.3.1 Heat Diffusion

The ISBA scheme, like most land surface models currently used in operational numerical weather prediction or general circulation model applications, considers that heat flow along the thermal gradient is the dominant first-order process and currently neglects other processes such as advection within the soil. Heat capacity (c) and thermal conductivity (K) are weighted averages of the respective volumetric proportions of air, rock, water, and ice (note that the latter is a difference from ISBA).

ISBA-DEB updates the temperature profile for the entire column each timestep using the heat equation in 1-dimension:

$$c_g \frac{\partial T_g}{\partial t} = \frac{\partial}{\partial z}\left[K \frac{\partial T_g}{\partial z}\right] \quad (1)$$

where K is thermal conductivity (W m^{-1}K^{-1}), c_g (J m^{-3}K^{-1}) volumetric ground specific heat capacity, z depth (m), and T_g ground temperature (K). Temperature in debris layers evolves not only by conductive heat transfer but also by latent heat from phase changes between water and ice in the debris (Φ, J m^{-3}s^{-1}) that is added to the right-hand side of equation 1, giving

https://doi.org/10.5194/tc-2019-168
Preprint. Discussion started: 10 September 2019

equation 2. These phase changes are calculated subsequently to the heat transfer routine; the temperature profile is updated accordingly as an adjustment at the end of the timestep (Figure 3).

$$c_g \frac{\partial T_g}{\partial t} = \frac{\partial G}{\partial z} + \Phi \tag{2}$$

In equation 2, conduction flux G represents the term in brackets on the right-hand side of equation 1. A 0 flux at depth provides the Neumann lower boundary condition, and surface flux from the energy balance provides the upper boundary condition. Shortwave radiation, longwave radiation, and turbulent fluxes together comprise the surface energy balance. We neglect energy carried by precipitation, an assumption supported by other work in the Himalaya (Azam et al., 2014) and on the nearby Tibetan Plateau (Huintjes et al., 2015).

ISBA-DEB calculates temperature for the snow-debris-ice column continuously. However, since the glacier cannot exceed 0 ^{o}C, we introduce a condition for the ice layers that follows an analogous scenario for snow in Boone and Etchevers (2001). Only the top layer of ice contributes to the glacier melt term. Underlying ice layers' temperatures are prevented from exceeding freezing by concentrating all above-freezing energy into the melt of the top ice layer. The top layer is 1 cm thick, far exceeding the melt possible in a single 15 minute timestep.

3.3.2 Glacier Melt

If the top layer of ice exceeds freezing, melt is computed and temperature reset to 0 ^{o}C. Sub-surface ice temperatures (i.e. layers 14–20) are subsequently recalculated with this 0 ^{o}C boundary condition, precluding melt from occurring in the sub-surface layers. Energy is conserved, and the amount of water melted in the top layer of the glacier in each timestep is added to the overlying debris and tracked for a cumulative annual ablation to compare with field measurements. The melting layer is implicitly refilled at the end of the timestep such that the 1 cm thick top layer begins every model iteration at full ice saturation.

3.3.3 Moisture Inputs and Diffusion

Water entering the debris from glacier melt and precipitation moves with a vertical flow rate F (m s^{-1}) and changes phase as a function of temperature. Mass leaves the system through latent heat mass fluxes and runoff (R). The amounts of liquid water (w_l) and ice (w_i), respectively, are given by

$$\frac{\partial w_l}{\partial t} = -\frac{\partial F}{\partial z} - \frac{\Phi}{L_m \rho_w} - \frac{S_l}{\rho_w} - \frac{R}{\rho_w} \qquad (w_{min} \leq w_l \leq w_{sat} - w_i) \tag{3}$$

$$\frac{\partial w_i}{\partial t} = \frac{\Phi}{L_m \rho_w} - \frac{S_i}{\rho_w} \qquad (0 \leq w_i \leq w_{sat} - w_{min}) \tag{4}$$

L_m is the latent heat of fusion (J kg^{-1}), ρ_w is the density of water, w_{sat} is the water concentration at saturation, and S_l and S_i are the source/sink terms (kg m^{-2}s^{-1}) for water and ice. Values of important physical constants and West Changri Nup glacier-specific parameters are listed in Table A1. A minimum water content $w_{min} = 0.0001$ is retained for numerical stability;

w_{min} in ISBA (0.001) was decreased by an order of magnitude in ISBA-DEB given the importance of the exact water content in heat and moisture diffusion calculations (Decharme et al., 2011; LeMoigne, 2018).

Vertical soil water flux is given by the Richards' equation and an additive term to account for water vapor. The Richards' equation is an expression derived from Darcy's Law that represents water diffusion arising from pressure gradients in partially saturated media.

$$\frac{\partial w_l}{\partial t} = \frac{\partial}{\partial z}\left[k(w_l)\left(\frac{\partial \psi}{\partial z}+1\right)\right] \tag{5}$$

Here, k (m s^{-1}) is hydraulic conductivity and ψ (m) is soil matric potential, the potential energy attributed to the adhesion of water to soil grains. In ISBA, vapor transport is addressed solely as diffusive; the hydraulic conductivity contains an additive term for vapor conductivity. There have been no observations of ice growth at the surface in subfreezing temperatures on West Changri Nup glacier (as on Mullins glacier, Antarctica by Kowalewski et al., 2011), suggesting that vapor is not a dominant transport mechanism and supporting the way it is included in ISBA for ISBA-DEB.

Adding the vapor transfer term to equation 5 gives

$$F = -k\frac{\partial}{\partial z}(\psi + z) - \frac{D_{v\psi}}{\rho_w}\frac{\partial \psi}{\partial z} \tag{6}$$

(Boone et al., 2000). $D_{v\psi}$ is the isothermal vapor conductivity (kg m^{-2}s^{-1}).

The Richards' equation (equation 5) includes both diffusion and drainage terms. Observations suggest that moisture transport in glacier debris is neither completely reservoir-like (as parameterized in Collier et al., 2014) nor fully governed by Darcy's Law (as in the original ISBA for soil) but rather some of both simultaneously. By solving the Richards' equation and using an appropriate hydraulic conductivity (Table A1), ISBA-DEB simulates both diffusion and pooling.

Moisture changes phase as a function of available mass and energy (Boone et al., 2000; Giard and Bazile, 2000). As soil freezes, ice is assumed to become part of the soil matrix such that ice lowers debris porosity and enhances the matric potential and vertical upward suction of water.

When there is ice in the debris, equation 6 is rewritten

$$F = -\kappa\frac{\partial \psi}{\partial z} - k \tag{7}$$

where $\kappa = \wp(k + \frac{D_{v\psi}}{\rho_w})$ and $\wp = 10^{-\alpha_\wp w_i/w}$ (Boone et al., 2000). $\wp$ is termed the "ice impedance coefficient," which inhibits upward movement of water towards the freezing front, and $\alpha_\wp$ is the "ice impedance factor," equal to 6 in ISBA (Johnsson and Lundin, 1991) and ISBA-DEB. The form of equation 7 emphasizes that there is a drainage term k and diffusion along a potential κ which includes isothermal vapor pressure.

The values of matric potential and hydraulic conductivity at saturation (ψ_{sat} and k_{sat}, respectively) are typically calculated according to Noilhan et al. (1995)'s continuous pedotransfer functions (PTFs), which compute key hydraulic parameters based upon soil composition. For PTF equations, see Appendix C1 of Decharme et al. (2011). Power curves of Brooks and Corey (1966) relate matric potential, hydraulic conductivity, and volumetric liquid water content to the variables computed by PTFs.

Instead of using a PTF to calculate k_{sat}, ISBA-DEB adopts gravel's k_{sat} value (0.03 m s^{-1}, Domenico et al., 1998) throughout the debris except for at the bottommost layer, where $k_{sat} = 0$ m s^{-1} (Table A1). This supplies a flux of 0 for the

https://doi.org/10.5194/tc-2019-168
Preprint. Discussion started: 10 September 2019

lower boundary condition, while rainfall and snowmelt provide the upper boundary condition. Equation 3 is solved with a Crank-Nicolson implicit time scheme.

3.3.4 Water Runoff

The pebble to gravel-sized grains comprising the debris cannot hold liquid water long-term, and water runs off (kg $m^{-2}s^{-1}$) with a slope-dependent timescale (Zuo and Oerlemans, 1996; Reijmer and Hock, 2008). The timescale is a linear function of glacier surface slope, with values of 1 h^{-1} for 0^o and 0 h^{-1} for 90^o (Collier et al., 2014) at the surface and an increasing value with depth. Runoff can be expressed as

$$R = \frac{w_j \rho_w \Delta z_j}{\tau_j} \left(\frac{\theta}{90} \right) \tag{8}$$

where θ is glacier surface slope, measured from horizontal, and z is the layer thickness (m). Runoff timescale τ_j must be $\leq dt$.

$$\tau_j = \tau_{min} + (\tau_{max} - \tau_{min}) \left[\frac{exp(\tau_\alpha \frac{z_j}{H}))}{exp(\tau_\alpha)} \right] \tag{9}$$

τ_α is a tunable shape parameter (Figure 4) defining the runoff timescale from its minimum value at the surface (1 hr, Collier et al., 2014) to its maximum value (also tuned) at the base of the debris, depth H (m).

https://doi.org/10.5194/tc-2019-168
Preprint. Discussion started: 10 September 2019

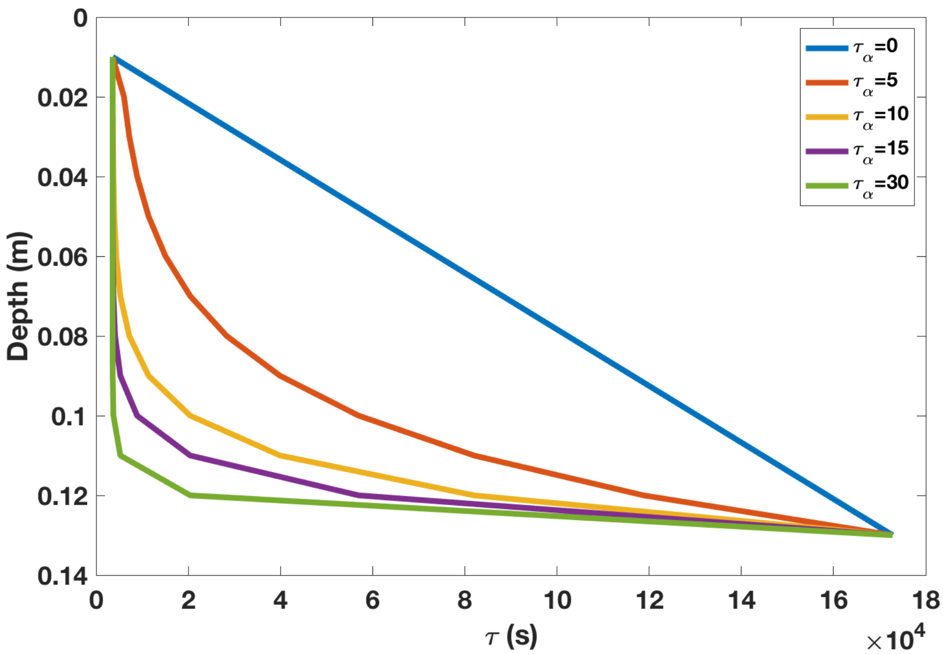

Figure 4. Timescale for lateral slope-induced runoff with the various timescale shape factors used in tuning. For all shape factors, the runoff timescale increases rapidly with depth.

This parameterization is necessarily simple in the absence of field measurements but corroborated by gravel's high hydraulic conductivity (Domenico et al., 1998) and the observed changes in debris' grain size distribution with depth. Debris grains tend to be smaller in size at the ice surface than at the top of the debris layer, thereby imparting more of a damming effect on entrained water lower in the debris column. The timescale of sand draining is on the order of a day or two (Blum et al., 2018), indicating an approximate magnitude to inform τ_{max} tuning tests. Further, debris permeability field tests show that after 10 s, $\sim 95\%$ of a 100 mL volume of water poured into gravel and cobbles drains. However, for fine particulates sampled at the ice interface (< 5 mm in diameter), only $\sim 20\%$ of the water drains in the same amount of time.

Since it takes a saturated sandy soil 24 – 48 hours to drain to its field capacity, 48 hours for τ_{max} is consistent with measurements of the kinds of particles at the base of a debris layer. A shape factor of 30 is consistent with observations of wetted debris right at the debris-ice interface (Nakawo and Young, 1981; Conway and Rasmussen, 2000; Nicholson and Benn, 2012). A $\tau_\alpha > 30$ does not change the shape of the runoff timescale (green curve in Figure 4) markedly, nor does it improve the RMSE significantly.

https://doi.org/10.5194/tc-2019-168
Preprint. Discussion started: 10 September 2019

Energy and water budgets in ISBA-DEB are the same as those in ISBA, with the exception of an additional term for glacier melt (M_{ice}). Both budgets close, and details are presented in the Supplementary Material.

4 Forcing

ISBA must be forced with a set of meteorological variables, a list of which can be found at *www.umr-cnrm.fr/surfex/spip.php?article215*.

4.1 In Situ Meteorological Measurements

The values of the meteorological forcing variables are supplied by field measurements at an AWS located at 5360 m a.s.l. on a 0.03 km^2 debris-covered area of West Changri Nup glacier (Sherpa et al., 2017; Vincent et al., 2016, dot in Figure 1). AWS data measured half hourly 6 December 2012 15:00 – 28 November 2014 13:30 local Nepal time provided all forcing data with the exception of CO_2 flux, which is merely assigned a reasonable value (6.2×10^{-4}) because ISBA-DEB is vegetation-free and insensitive to it. Measurements at the AWS also included half hourly ablation readings and debris temperatures. During the December 2012 – November 2014 period used for this study, there were four thermistors giving debris temperatures at distributed depths. Field campaigns supplied additional measurements of debris density and porosity, and precipitation was measured at nearby Pyramid Research Station. Table 2 summarizes available data from these stations, some of which (Figure 5) drives the model.

4.2 Precipitation

The nearest direct measurement of precipitation is from a Geonor T200B all-weather sensor at Pyramid Research Station (5035 m a.s.l., 4.3 km from the AWS). Sherpa et al. (2017) contains details on the precipitation dataset, which begins 6 December 2012. In our study, we assumed corrected total precipitation at Pyramid Research Station equivalent to total precipitation on West Changri Nup glacier. Because of differences in elevation and local microclimates, we repartitioned phase based on AWS local temperature following Wagnon et al. (2009), with subsequent minor adjustments based on SR50 measurements.

https://doi.org/10.5194/tc-2019-168
Preprint. Discussion started: 10 September 2019

The Cryosphere Discussions
Open Access

Quantity	Data Gaps (%)	Instrument	Accuracy according to the manufacturer
West Changri Nup AWS (5360 m a.s.l.):			
Air temperature* § (^{o}C)	24	Vaisala HMP45C	$\pm0.2^o$C
Relative humidity* § (%)	24	Vaisala HMP45C	$\pm2\%$
Wind direction (^{o}) and speed § (m s^{-1})	43	Young 05103-5	$\pm3^o$ and ±0.3 m/s
Incident shortwave radiation § (W m^{-2})	18	Kipp and Zonen CNR4 [$0.305 < \lambda < 2.8\mu$ m]	$\pm3\%$
Reflected shortwave radiation § (W/ m^{-2})	18	Kipp and Zonen CNR4 [$0.305 < \lambda < 2.8\mu$ m]	$\pm3\%$
Incoming longwave radiation § (W m^{-2})	24	Kipp and Zonen CNR4 [$5 < \lambda < 50\mu$ m]	$\pm3\%$
Outgoing longwave radiation § (W m^{-2})	24	Kipp and Zonen CNR4 [$5 < \lambda < 50\mu$ m]	$\pm3\%$
Debris temperature # (^{o}C)	24	TCA PT100	$\pm0.1^o$C
Ablation/accumulation (m)	33	Campbell SR50	±1 cm
Pyramid Research Station (5035 m a.s.l.):			
Precipitation (mm w.e.)	0	Geonor T200B	±0.1 mm

Table 2. Meteorological quantities and debris characteristics measured by the AWS on West Changri Nup glacier 6 December 2012 9:15 – 28 November 2014 7:45 UTC. All sensors give values every 30 minutes; these values are 30 minute averages of data with 30 second scanning intervals for all values except the ultrasonic SR50 and wind direction, which are sampled every 30 min. An * indicates measurements that must be gathered with artificial aspiration in the daytime, a § denotes quantities used to drive ISBA-DEB, and a # marks variables used for assessing model performance. Precipitation was measured at Pyramid Research Station hourly until 16 May 2016 8:15 UTC and half-hourly after that time.

https://doi.org/10.5194/tc-2019-168
Preprint. Discussion started: 10 September 2019

The Cryosphere
Discussions
Open Access

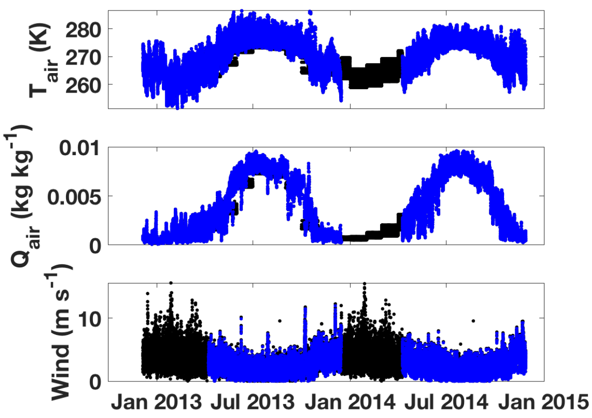

(a)

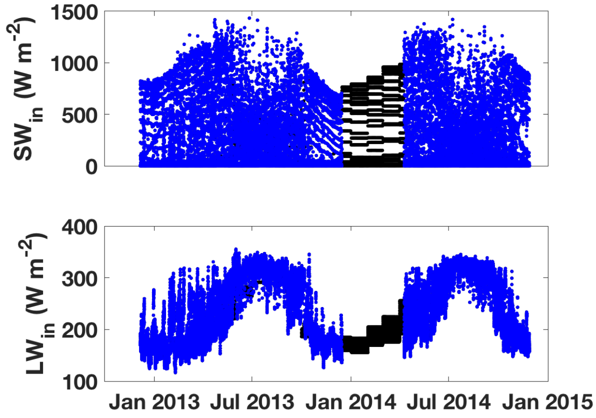

(b)

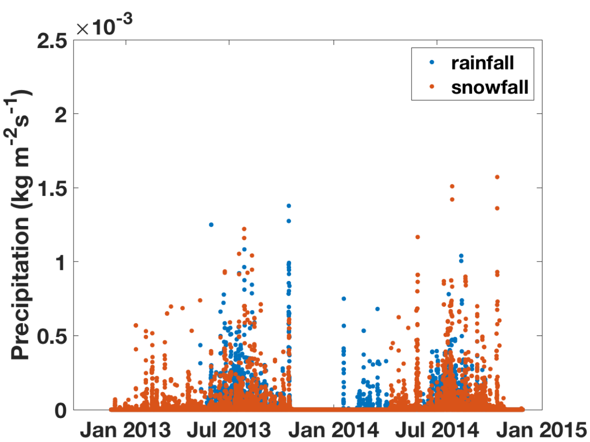

(c)

Figure 5. (a–b) Continuous half-hourly forcing data in black, with *in situ* data overlaid in blue. The gaps are apparent where the black data points are displayed; Section 4.3 describes the procedure used to assign these values. (c) The continuous precipitation dataset from Pyramid, with phase partitioned by T_{air} at West Changri Nup glacier (top panel of a).

https://doi.org/10.5194/tc-2019-168
Preprint. Discussion started: 10 September 2019

4.3 Gap-filling

The two-year period used in this study contains data gaps of various lengths affecting different sensors (see Table 2). For example, a battery problem prevented nighttime data readings between April and December 2013 (Figure 6), installation problems made the wind readings questionable for several months, and station tilt compromised the quality of some measurements but not others. Because the forcing file for SURFEX must be continuous, it was necessary to fill such data gaps and periods when data was deemed suspect. See the portion of data plotted with black in Figures 5a and b and the % data gaps in Table 2 for the extent of missing AWS data over the period used in this study.

Missing meteorological values were approximated by the monthly averages of values at the missing timestep during a longer period of data acquisition at the AWS than used for this study: October 2010 – November 2016. Every missing value was filled with the corresponding time step's mean monthly value. Using values specific to timestamps preserved both diurnal and seasonal variability in the gap-filled dataset. This method proved inappropriate for wind speed, whose amplitude and variability could not be conserved with averages. For the whole series, the wind speed data are gap-filled by the wind speed at the same timestamp in a different year of the AWS's operation, randomly selected. When the same timestamp in all years is missing a wind speed, we choose the closest later timestamp with data in any year.

5 Tuning

Of the December 2012 – November 2014 series used in this study, we used 2014 debris temperatures to tune parameters and 2013 ablation to assess the impact of moisture inclusion in ISBA-DEB. We compared simulated debris temperatures with measured ones April 9, 2014 – November 28, 2014 (Figure 6), using an RMSE calculation to capture the magnitude of temperature. We tested five runoff timescale shape factors (τ_α, Figure 4) and maximum runoff timescale (τ_{max}) values of 3, 6, 18, 24, 48, 72, and 96 hours. The RMSE metric suggested τ_α =30 and τ_{max} =48; however, the actual error values for these were not dramatically different from those for the other values of τ_α and τ_{max}. We used τ_α =30 and τ_{max} =48 for our modeling work, despite shallow minima, because they are highly plausible values.

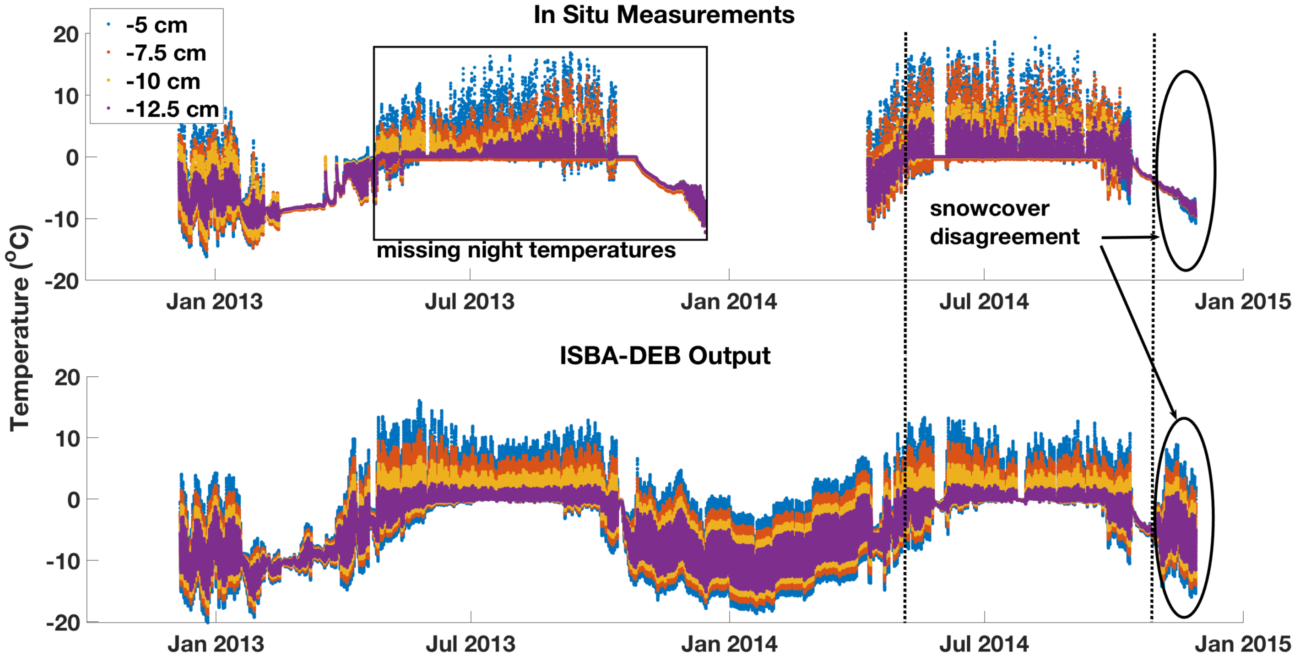

Figure 6. Measured (upper panel) and modeled (lower panel) debris temperatures at depths of 5 cm, 7.5 cm, 10 cm, and 12.5 cm. The model runs were carried out with $\tau_\alpha = 30$ and $\tau_{max} = 48$ hr. The period between the vertical dashed lines, April 9, 2014 – November 28, 2014, was most informative for comparison because there was a battery problem causing no nighttime temperature recordings April – December 2013 (period indicated by the black box), and the clear temperature disagreement in late 2014 results from a problem in the meteorological forcing file for ISBA-DEB (having insufficient snowfall to produce the observed persistent snowcover).

6 Results and Discussion

In this section, we present the results (and describe the behaviour) of model simulations for nearly two years of meteorological forcing, describe key physical processes related to the presence of debris, and show results from a series of sensitivity tests related to parameter uncertainties.

https://doi.org/10.5194/tc-2019-168
Preprint. Discussion started: 10 September 2019

6.1 Model Simulation Characteristics

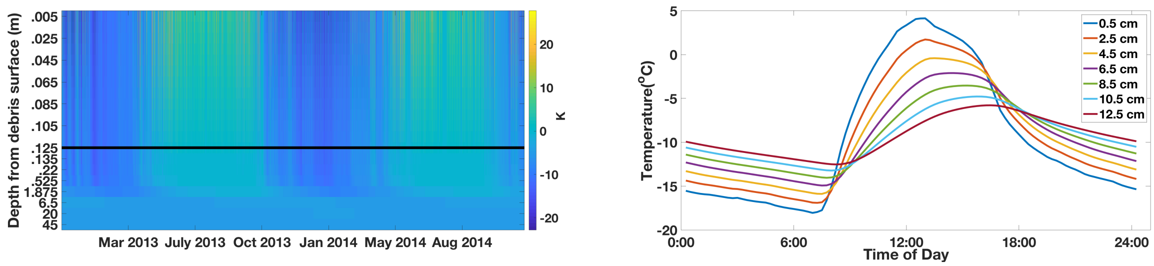

(a) (b)

Figure 7. (a) Temperatures in debris (top 12.5 cm) and underlying glacier (which extends to 60 m and is below the black line indicating the ice-debris interface) throughout the period used for this study; y-labels correspond to the mid-layer depth of the 20 discrete layers used in ISBA-DEB (note non-linear y-scale). The temperatures simulated throughout the whole 60 m column over the entire forcing period show phase lag and attenuation with depth, characteristics that are more clearly seen in (b), which shows the temperature of various debris depths during an arbitrary day (20 February 2014).

During the model simulations, glacier melt, snowmelt, and rain enter the debris base or surface. The moisture in each layer evolves with time, and the phase of the moisture changes as a function of temperature. Supplementary Figure A2 illustrates debris water input in the top (surface) and bottom (glacier interface) panels. Its middle four panels show how the liquid and solid moisture contents change with temperature in the top two and bottom two layers of debris (i.e. layers 1, 2, 12, and 13). ISBA-DEB simulates temperature evolution throughout the entire debris-glacier model domain (Figure 7a); the domain is 60 m total, including the 13 debris layers, each 1 cm thick. Output shows temperature amplitude attenuation and phase lag with depth (clearly seen in Figure 7b). Above-freezing temperatures propagating into the ice cause melt (Figure 8).

https://doi.org/10.5194/tc-2019-168
Preprint. Discussion started: 10 September 2019

The Cryosphere
Discussions

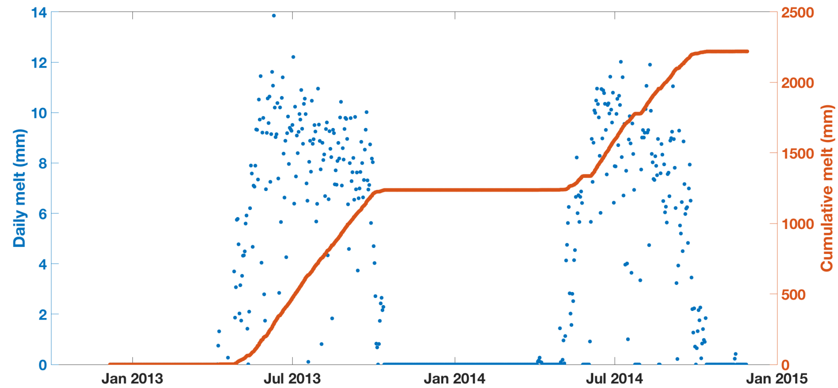

Figure 8. Daily totals of glacier melt (blue dots), overlaid by cumulative melt (red line) over the entire period December 2012 – November 2014.

As the debris' moisture content and phase vary, its thermal conductivity and heat capacity evolve accordingly (Figure 9; extreme values are listed in Table 1). The temporal and spatial evolution of these parameters throughout the debris column as a function of water and ice contents is a strength of ISBA-DEB.

https://doi.org/10.5194/tc-2019-168
Preprint. Discussion started: 10 September 2019

The Cryosphere
Discussions
Open Access

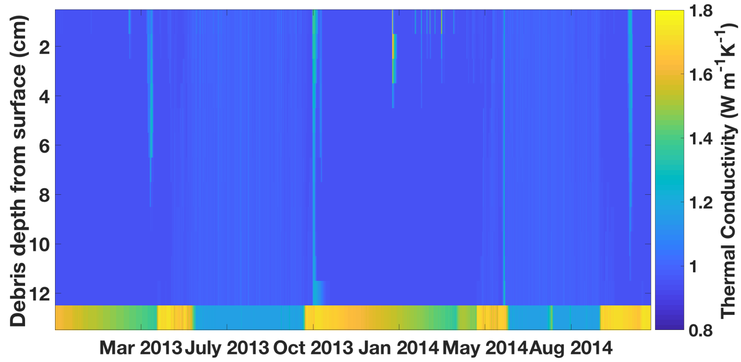

(a)

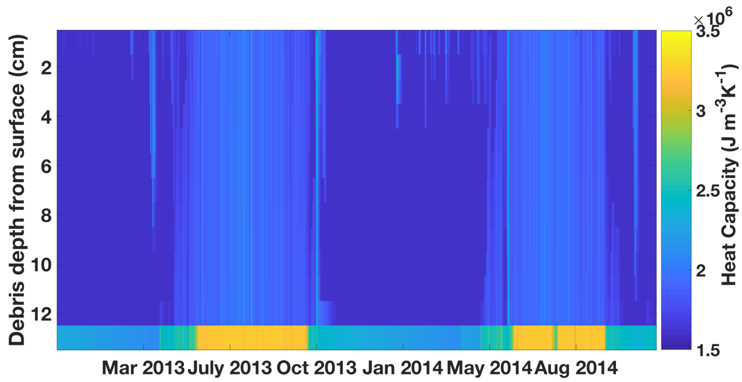

(b)

Figure 9. Temporal evolution of (a) thermal conductivity and (b) volumetric heat capacity according to debris moisture amount, phase, and gradient in the top and bottom layers of debris. Layers 1 – 12 look similar because the moisture is concentrated in layer 13, which is just above the ice-debris interface.

6.2 Wet versus Dry Debris

We ran an experiment to contrast the sub-debris melt under totally dry, partially saturated, and fully saturated debris layers forced with the same meteorological conditions measured on West Changri Nup glacier between December 2012 and November 2014 (Section 4). The "partially saturated" scenario uses parameters listed in Table A1. Figure 10 shows the three computed ablation values for 2013 and the value measured from an ablation stake the same year.

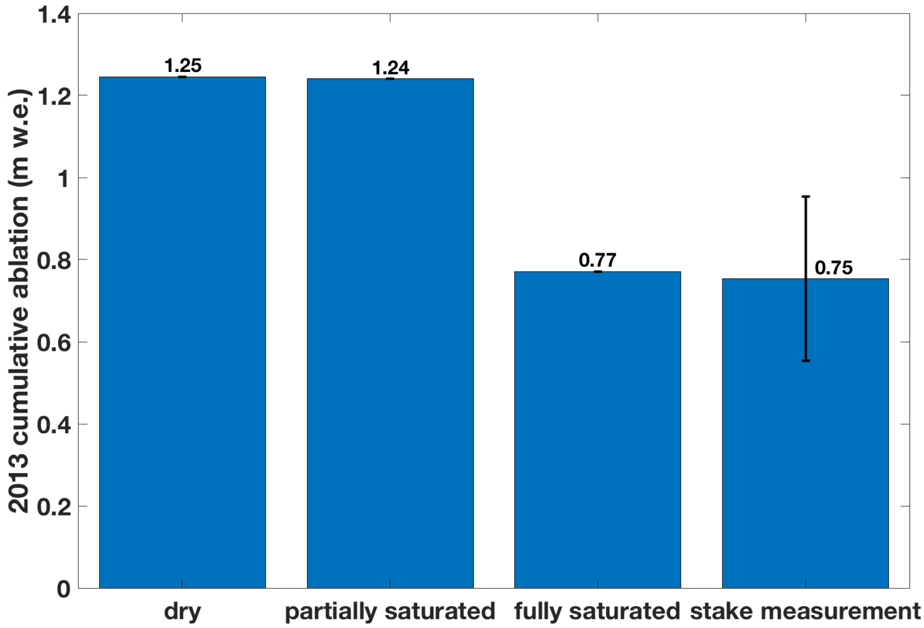

Figure 10. Annual cumulative ablation of three model runs (dry debris, partially saturated debris, and fully saturated debris) compared with measured ablation of 2013; model output for 2014 is similar. Note that the measurement comes from a single ablation stake and has an uncertainty of ± 20 cm w.e. (Vincent et al., 2016).

The glacier under completely dry debris melts significantly more than the glacier situated under saturated debris. Sub-debris melt is a function of the debris thickness, which is the same for all three cases, and the thermal diffusivity of the debris (K/c_g in equation 1), which differs for all three as a function of the amount, phase, and location of moisture. Completely water-saturated debris has a thermal diffusivity that is less than half of the diffusivity for completely ice-saturated debris. Dry debris' diffusivity falls nearly midway between the two (Table 1). The share of water and ice in the interstitial spaces of the partially (Figure 11a) and fully (Figure 11b) saturated debris differs significantly in amount and distribution. Ice-saturated debris conducts heat much more efficiently than water-saturated debris does; however, glacier melt happens only when the glacier surface exceeds 0 ^{o}C, and efficiently conducting, ice-laden debris overlying a melting glacier is a physical impossibility.

https://doi.org/10.5194/tc-2019-168
Preprint. Discussion started: 10 September 2019

The Cryosphere Discussions

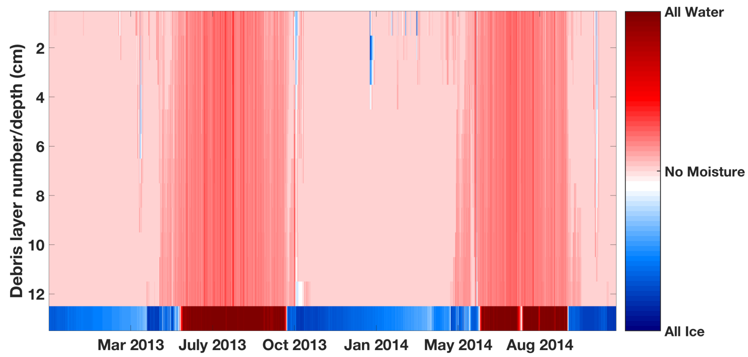

(a)

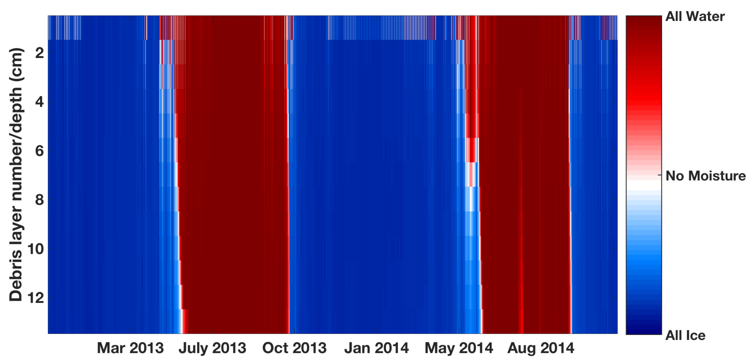

(b)

Figure 11. Debris layer moisture by phase in (a) the partially saturated ISBA-DEB and (b) the fully saturated ISBA-DEB scenarios. As shown in (b), the fully saturated debris is water-filled (having a lower thermal diffusivity than dry debris) during the summers when debris surface temperatures lead to glacier melt. The difference in moisture in the debris surface layer accounts for the different latent heat fluxes (Figure 12).

https://doi.org/10.5194/tc-2019-168
Preprint. Discussion started: 10 September 2019

The Cryosphere Discussions
Open Access
EGU

The surface latent heat flux is much greater over the saturated debris, and the latent heat flux due to phase changes within the debris is also greatest for the saturated debris (Figure 12). Energy used for evaporation and sublimation leaves comparatively little energy for heat conduction through the ice-debris interface.

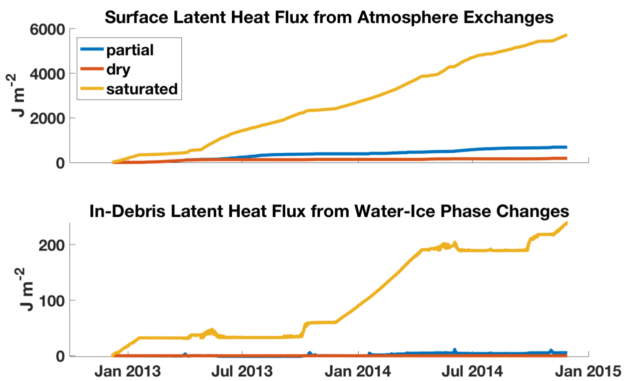

Figure 12. Cumulative heat fluxes related to the sub-debris ablation of the three scenarios (dry debris, partially saturated debris, and fully saturated debris). The surface latent heat flux exchanged with the atmosphere (upper panel) indicates how much energy is removed from the system at the debris surface, while the latent heat from phase changes within the debris (lower panel) shows how much energy is removed from the system in the sub-surface of the debris layer. A greater latent heat flux corresponds to a lower conductive heat flux through the debris into the underlying glacier.

Overall, our results show that including debris moisture in ISBA-DEB over 2012 – 2014 on West Changri Nup glacier does not significantly decrease sub-debris glacier melt. The expected reduction in melt under partially saturated debris has a magnitude determined by the distribution and amount of water in the debris; thus, the amount of melt is highly sensitive to the runoff parameterization, the assumptions made in the construction of ISBA-DEB, and the meteorological forcing. The partially saturated debris is predominantly dry, with the exception of the lowermost layer (Figure 11a). With different runoff parameters and/or more water entering the debris from precipitation, partially saturated debris could yield an annual ablation closer to the value for saturated debris in Figure 10. Additionally, ISBA-DEB follows ISBA's calculation of atmospheric latent heat exchange from the top layer only. Introducing an atmospheric latent heat flux within the debris similar to that at the "saturated horizon" of Collier et al. (2014) would give lower glacier melt underlying a partially saturated debris layer. This is discussed further in Section 6.5.

Our results are consistent with the work of Reid and Brock (2010), who showed that sub-debris melt decreased with the incorporation of latent heat flux in their model. Including latent heat fluxes in their model when the relative humidity equaled 100% produced a better fit between model output and measurements. Collier et al. (2014) showed that incorporating moisture in a debris energy balance model decreased melt calculations but that surface fluxes either may or may not compensate, giving a positive or negative total mass balance depending on meteorological conditions. We present cumulative flux used for melt along with cumulative surface and in-debris latent heat fluxes in Figure 12. Our partially saturated glacier melts 44 mm less

https://doi.org/10.5194/tc-2019-168
Preprint. Discussion started: 10 September 2019

than the dry one in 2013 but loses 105 mm w.e. through surface latent fluxes (152 mm w.e. with snow sublimation added to latent heat mass loss from the glacier ice only). In 2013, the latent heat mass flux more than compensates for the reduction in icemelt such that the system with a partially saturated debris layer loses more net mass than a system with a dry debris layer.

6.3 Sensitivity Tests

We performed sensitivity tests on the six parameters listed in Table 3. In most cases, the tested ranges were informed by literature. In the case of albedo, which has been found to vary up to 0.6 on debris-covered glaciers in the Everest region (Kayastha et al., 2000), we tested values ranging from 0.1 – 0.5; Kayastha et al. (2000) claimed that most albedo values fall in the 0.2 – 0.4 range, while Nicholson and Benn (2012) showed that 62% of their measurements fell between 0.1 and 0.3. A mid-day mean of the ratio of reflected to incoming shortwave radiation measured on West Changri Nup glacier gives an albedo of 0.2. Despite the fact that albedo has been measured on West Changri Nup glacier, ISBA-DEB's sensitivity to this parameter is important to assess for future application of ISBA-DEB to other debris covers.

A study on Miage glacier, Italy provided 0.94 W m^{-1}K^{-1} as a starting point for thermal conductivity tests (Reid and Brock, 2010), though we varied the conductivity values throughout the range reported in the literature, 0.60 to 1.29 W m^{-1}K^{-1} (Rounce et al., 2015).

Aerodynamic roughness lengths are used to determine the two exchange coefficients (C_H, C_D) in the stability correction for the bulk method of calculating turbulent heat fluxes (i.e. fits to the Monin-Obukhov functions, see Noilhan and Mahfouf, 1996). C_D (for momentum) depends on $z_{0,m}$, while C_H (for H and LE) depends on both $z_{0,m}$ and $z_{0,h}$. The surface roughness length due to momentum, $z_{0,m}$, is the height above a rough surface at which the horizontal wind speed is zero. It varies with time and snowfall, and it is notoriously poorly constrained (Quincey et al., 2017) and difficult to compute consistently with different approaches (Miles et al., 2017). Because their values are inherently difficult to measure and poorly known, roughness lengths are dependent upon not only the local surface state but also meteorology and surrounding surface features. Studies that informed our range of tested values were: Inoue and Yoshida (1980) and Takeuchi et al. (2000) for 0.0035 m and 0.0063 m on Khumbu glacier, respectively; Reid and Brock (2010) for 0.016 m on Miage glacier; and Lejeune et al. (2013) for 0.05 m determined through model tuning on West Changri Nup glacier. We test 0.1 m, reasoning that debris' roughness can be approximated by that of rough ice (Smeets and Van den Broeke, 2008). An upper end member, 0.5 m, is taken from Miles et al. (2017)'s value for boulders on Lirung glacier. Their value for gravels (0.005 m) and Quincey et al. (2017)'s recent measurements at two sites on Khumbu glacier (0.0184 and 0.0243 m) fall within the range of tested values.

The roughness length of heat transfer ($z_{0,h}$) is incorporated into ISBA through the variable $z_{0,m}/z_{0,h}$, which must be ≥ 1. The smaller this ratio, the larger $z_{0,h}$ and the larger C_H (and turbulent flux). $z_{0,m}/z_{0,h}$ is commonly taken to be $= 10$ (ISBA default, Mascart et al., 1995), but we test a wide range for ISBA-DEB given the uncertainty surrounding the value of this parameter. We test ratio values of 1, 4, 7, 10, 25, 50, 100, and 200.

Emissivity affects net longwave radiation and other surface fluxes through feedbacks; we test the model's response to a wide range of values for this parameter (i.e. 0.9 – 1). Finally, we test how sensitive model-simulated ablation is to the user-specified slope that determines runoff. We test a range from flat to a slope of 10^o. Figure 13 summarizes cumulative melt over the entire

https://doi.org/10.5194/tc-2019-168
Preprint. Discussion started: 10 September 2019

Parameter	Cumulative Ablation (mm) Dec. '12 – Nov. '14	% Change (relative to *)
albedo (α)=0.1	2425.10	9.25
albedo (α)=0.2*	2219.80	-
albedo (α)=0.3	2001.10	-9.85
albedo (α)=0.4	1766.60	-20.42
albedo (α)=0.5	1510.40	-31.96
th. cond. (K)=0.6W $m^{-1}K^{-1}$	1533.30	-30.93
th. cond. (K)=0.7W $m^{-1}K^{-1}$	1760.80	-20.68
th. cond. (K)=0.8W $m^{-1}K^{-1}$	1966.20	-11.42
th. cond. (K)=0.94W $m^{-1}K^{-1}$*	2219.80	-
th. cond. (K)=1.0W $m^{-1}K^{-1}$	2317.20	4.39
th. cond. (K)=1.1W $m^{-1}K^{-1}$	2466.40	11.11
th. cond. (K)=1.2W $m^{-1}K^{-1}$	2603.10	17.27
th. cond. (K)=1.3W $m^{-1}K^{-1}$	2730.70	23.02
mom. rough. l. ($z_{o,m}$)=0.0035m	3081.90	38.84
mom. rough. l. ($z_{o,m}$)=0.0063m	2879.50	29.72
mom. rough. l. ($z_{o,m}$)=0.016m	2575.20	16.01
mom. rough. l. ($z_{o,m}$)=0.05m*	2219.80	-
mom. rough. l. ($z_{o,m}$)=0.1m	2008.40	-9.52
mom. rough. l. ($z_{o,m}$)=0.5m	1502.30	-32.32
th. rough. l. ($z_{o,h}$)=0.05m	1426.20	-35.75
th. rough. l. ($z_{o,h}$)=0.0125m	1945.70	-12.35
th. rough. l. ($z_{o,h}$)=0.0071m	2115.30	-4.71
th. rough. l. ($z_{o,h}$)=0.005m*	2219.80	-
th. rough. l. ($z_{o,h}$)=0.002m	2479.60	11.70
th. rough. l. ($z_{o,h}$)=0.001m	2663.30	19.98
th. rough. l. ($z_{o,h}$)=0.0005m	2827.60	27.38
th. rough. l. ($z_{o,h}$)=0.0003m	2949.70	32.88
emissivity (ϵ)=0.9	2246.90	1.22
emissivity (ϵ)=0.94*	2219.80	-
emissivity (ϵ)=1	2179.90	-1.80
slope= 0^o	1479.40	-33.35
slope= 1^o	1539.90	-30.63
slope= 2^o	1694.30	-23.67
slope= 3^o	1908.20	-14.04
slope= 4^o	2094.60	-5.64
slope= 5^o*	2219.80	-
slope= 6^o	2284.30	2.91
slope= 10^o	2320.40	4.53

Table 3. Summary of sensitivity tests performed on ISBA-DEB. An asterisk indicates values that are used in Section 6.1 and for the partially saturated scenario in Section 6.2. These values provide the basis of comparison in column 3.

two year period for the extreme parameter values tested, and Supplementary Figure A3 shows cumulative melt for all parameter values in Table 3.

https://doi.org/10.5194/tc-2019-168
Preprint. Discussion started: 10 September 2019

The Cryosphere Discussions

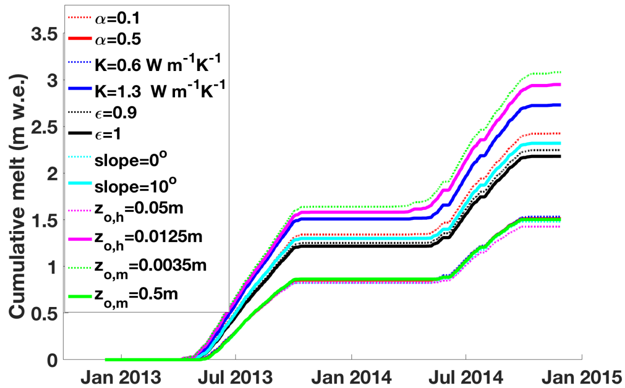

Figure 13. Cumulative glacier melt over the December 2012 – November 2014 period under the extreme values for each parameter listed in Table 3. An equivalent figure for each parameter may be found in the Supplementary Material (Figure A3).

As shown in the subplots of Supplementary Figure A3 and associated Table 3, the ISBA-DEB model would give significantly different melt results on glaciers with a much more reflective debris cover (i.e. a lithology with a higher albedo), a much flatter surface, or different $z_{0,m}$ and $z_{0,h}$ values. Sensitivity is analyzed further in Section 6.4 on Uncertainty.

Given the responsiveness of ISBA-DEB's calculated ablation to thermal conductivity, we elected to compare simulated and measured debris temperatures to glean information about which value of thermal conductivity yields simulated debris temperatures that most closely match measured ones in timing (via R^2 of envelope functions) and magnitude (via RMSE). Our tests do suggest an optimal value of 1 W $m^{-1}K^{-1}$, which agrees closely with that of Reid and Brock (2010), though further tests over more time periods with available debris temperatures are necessary because neither of these tests yielded deep minima.

Figure 14 accompanies Supplementary Figure A3 in that it shows which energy flux is most impacted by the complementary sensitivity tests; it shows which energy fluxes have the strongest impact on the variation of the cumulative melt curves shown in Supplementary Figure A3.

https://doi.org/10.5194/tc-2019-168
Preprint. Discussion started: 10 September 2019

The Cryosphere
Discussions
Open Access

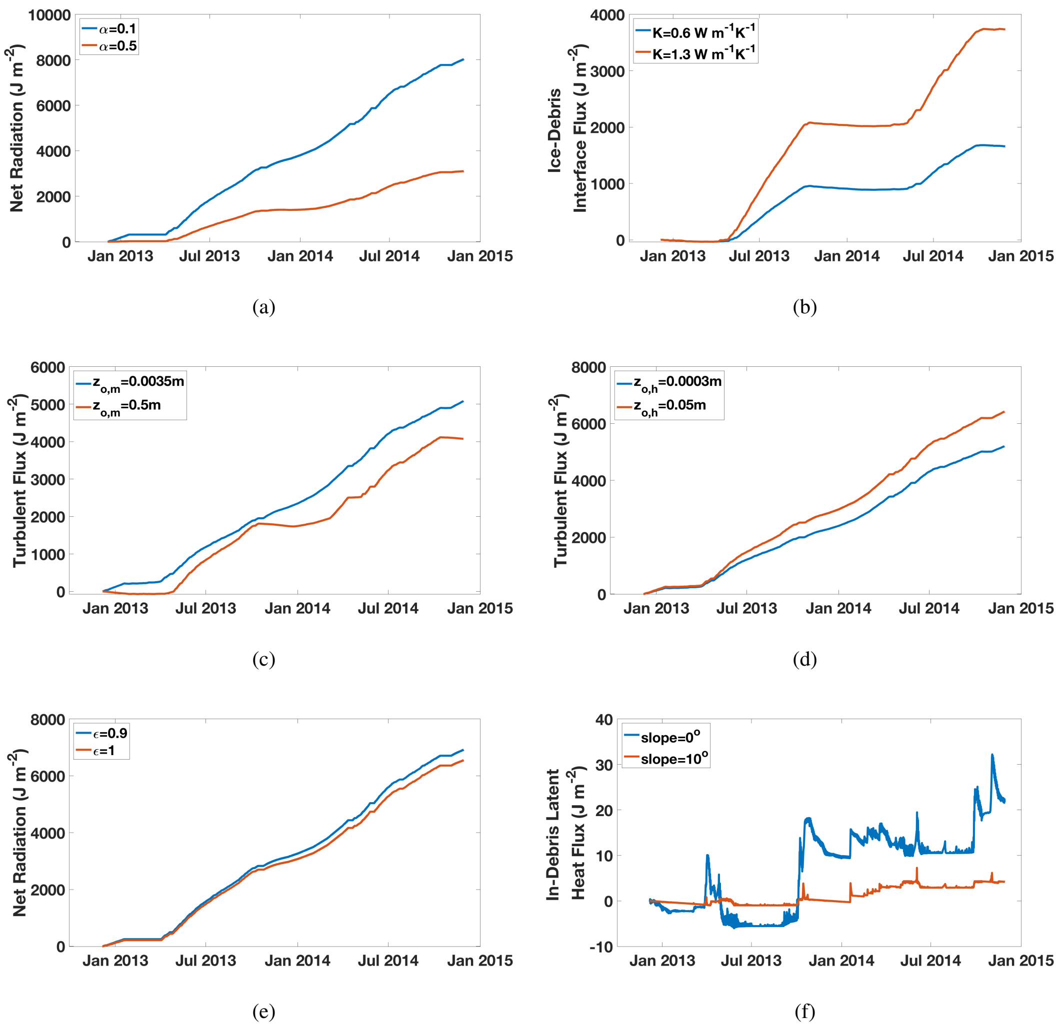

Figure 14. Cumulative energy fluxes most impacted by the six parameters perturbed through sensitivity tests, shown with the maximum and minimum tested values. Subfigure locations correspond to Supplementary Figure A3.

https://doi.org/10.5194/tc-2019-168
Preprint. Discussion started: 10 September 2019

Roughness lengths and slope affect the latent heat fluxes the most. Because the slope affects the residence time of water in the debris, it affects the flux of latent heat due to phase changes within the debris. Changes in albedo and emissivity affect the net shortwave and longwave radiation fluxes, respectively, and their effects are shown on the net radiation. Thermal conductivity, by definition, has the greatest impact on the conductive heat flux, the cumulative value of which varies from 1657.78 J m^{-2} for K = 0.6 W $m^{-1}K^{-1}$ to 3734.44 W m^{-2} for K = 1.3 W $m^{-1}K^{-1}$.

Our simulations showed that sensible heat flux (H) is one order of magnitude larger during the monsoon and a factor of seven larger during the pre- and post-monsoon than that measured using an eddy correlation approach over Lirung glacier (Langtang area, Nepal, 4250 m a.s.l., Steiner et al., 2018). Although the sites differ in topography, meteorology, and elevation and are, thus, not fully comparable, we suspect that sensible heat flux is overestimated by ISBA-DEB on West Changri Nup glacier. Since $H = \rho_{air} * C_p * C_H * V * (T_{surf} - T_{air})$, where C_p is heat capacity and V wind speed, an anomalously large H implies that the surface debris in ISBA-DEB is overheating and evacuating too much heat. Some decrease in sensible heat magnitude was achieved through adjusting the roughness lengths and albedo, although further work is necessary to improve the sensible heat flux calculated by ISBA-DEB when the simulated surface temperature is greater than the prescribed air temperature for an extended period (i.e. during unstable conditions). Because an excessively large sensible heat flux removes heat from the debris that could otherwise be put towards glacier melt, resolving the sensible heat overproduction would likely lead to an increase in ISBA-DEB's glacier melt calculation.

The sensible heat flux magnitude simulated by ISBA-DEB could be due to a number of underlying factors that provide avenues for future investigation. First, both the sensitivity tests and disagreement of ISBA-DEB's sensible heat magnitude and that of Steiner et al. (2018) suggest that $z_{o,m}$ =0.05 m and $z_{o,h}$ =0.005 m are not spatially representative values. Additionally or alternatively, processes missing from ISBA-DEB could influence H. ISBA-DEB's lack of advection and its highly simplified vapor transport (rather than empirical fit to Monin and Obukhov (1954)'s curves) may account for the anomalously large H. Finally, we assume our observed energy fluxes comprise a closed budget, a condition that ISBA follows, but we cannot rule out that energy budget errors in observations contribute to the large H magnitude without a detailed future evaluation. Robust assessment of H over debris covered glaciers requires more measurements using eddy correlation.

6.4 Uncertainty

Although slope is known for West Changri Nup glacier's AWS, the slope at other sites where ISBA-DEB could be applied will inevitably vary. A slight change in surface slope, particularly if the slope is less than 5^o, has a dramatic impact on the sub-debris melt calculated by ISBA-DEB. Runoff is directly proportional to slope angle such that a greater slope indicates more runoff and less potential for water buildup and turbulent heat exchange. A flatter slope gives a more water-saturated debris layer, and it's useful to make a comparison between the model runs with various slope values and model runs with dry vs saturated debris. For slopes higher than 5^o, the debris is drained sufficiently well that it is no longer dominated by the thermal properties of water. Sub-debris ablation on a slope of 0^o – 4^o somewhat resembles that under fully saturated debris, with the flat slope's debris having a lower interface flux and higher surface latent heat flux than the more sloped and comparatively drier debris. The flat debris does not show nearly the same magnitude of surface latent heat as the saturated debris does; while its top layer

https://doi.org/10.5194/tc-2019-168
Preprint. Discussion started: 10 September 2019

has more moisture than the debris overlying flatter glaciers, it is far from fully saturated. The configuration that holds more water in the debris has a greater in-debris latent heat flux (Figure 14f, like the lower panel of Figure 12).

In order for ablation computed by ISBA-DEB to be within 10% of true ablation, albedo must not vary by more than ± 0.1 and the conductivity should stay within ± 0.15 W m^{-1}Km^{-1}. Table 3 shows the model sensitivity to roughness lengths and emphasizes the need to verify a site-specific value before applying ISBA-DEB at that different site. The varied measurements (2/3 on neighboring Khumbu glacier) increase model ablation by 16, 30, and 39% over two years, respectively, while the theoretically-reasoned greater roughness length decreases it by nearly 10% and Miles et al. (2017)'s value for boulders by over 30%. The thermal roughness length is even more poorly constrained than the roughness length for momentum, and our tests simply explored model response to a range of ratios. They demonstrate how crucial this parameter, which determines calculated latent heat fluxes, is to an energy balance model. Losing more energy to latent heat leaves less for glacier melt. Increasing the ratio from 10 to 25 increases ablation by more than 10%.

Measured ablation over the two years modeled is 75.3 ± 20 cm (2012 – 2013) and 47.1 ± 20 cm (2013 – 2014). The measured ablation carries with it great uncertainty (above we use ± 20 cm from Vincent et al., 2016), as do the depths of the temperature sensors within the debris. The four thermistors were installed at depths of 5, 7.5, 10, and 12.5 cm in 12.5 cm of debris in December 2012. Before the end of their deployment in November 2014, their depths were checked and reset only twice: December 2013 and April 2014. Therefore, while a portion of the modeled-measured temperature mismatch is due to the inability of ISBA-DEB to represent the system perfectly, another portion is due to the migration of the thermistors in the debris, which renders their depths unknown. It is not possible to attribute the disagreement of ISBA-DEB temperatures with measured ones entirely to the model.

6.5 Future Directions

A central part of the ISBA structure is the neglect of advection based on the observation that advective heating makes relatively small changes to the soil temperature compared to conduction. In addition to the thermal properties, hydraulic properties, and hydrological processes accounted for in ISBA-DEB, soil and debris also differ in the size of their interstitial void spaces. In highly permeable debris, there is ample space for air flow through the debris layer. Advective heat transfer is not accounted for in ISBA or ISBA-DEB.

Reznichenko et al. (2010) showed in a laboratory that rain advects heat from warm, highly permeable debris to the glacier surface. Sakai et al. (2004) showed that heat flux from percolated water assigned the temperature of debris was only 9% of the icemelt flux despite the fact that 75% of rainfall percolated, whereas the evaporative flux equaled nearly half of the net radiative flux, the main driver of glacier melt. They concluded that not accounting for the evaporative heat flux would lead to a twofold overestimation of sub-debris melt. They also pointed out, in comparing their two sites of data collection, that, in contrast to soil, supraglacial debris has a higher permeability and lower evaporation rate. A lower evaporation rate is consistent with the fact that debris stores moisture at depth. Moisture deep in debris is less prone to evaporation – although some does evaporate – than moisture on the surface.

https://doi.org/10.5194/tc-2019-168
Preprint. Discussion started: 10 September 2019

The Cryosphere Discussions

Evatt et al. (2015) designed a model that was novel in its incorporation of the evaporative heat flux at the bottom of the debris layer. They justified their parameterization by noting that the melt occurs at the debris base and pointed out that calculating evaporation lower in the debris requires accounting for the air flow within the debris. Significant air flow is absent in soils for which the original ISBA was designed. By adjusting the surface vapor pressure term based upon the water content in the debris, Collier et al. (2014) also considered the latent heat flux within the debris layer.

Evaporative heat fluxes in ISBA are computed based on moisture content of only the top layer. While such a parameterization of the evaporative heat flux may be reasonable in soils, it has no physical basis in far more permeable debris, within which the atmosphere can exchange heat and mass at different depths. Collier et al. (2014) found that the latent heat flux calculated at the saturated horizon of their reservoir model was too low, offering that their computed saturated horizon itself was flawed without accounting for capillary effects. Therefore, ISBA-DEB provides an advancement in prognosing the location of moisture, which both pools (as in Collier et al. (2014)'s model) and undergoes diffusion. Introducing the possibility for latent heat fluxes to arise from within the debris is the next step in furthering ISBA-DEB.

7 Conclusions

While the introduction of advective heat transfer and atmospheric exchanges deeper than the surface of the debris could make the model more physically realistic, ISBA-DEB nevertheless provides an advancement in modeling the processes in a debris layer. It is the first model to integrate heat conduction with moisture diffusion – and has the capability of representing partially saturated debris year round, even when the ice temperature is subfreezing and a snowpack is present on the debris. It reasonably simulates the temperature evolution of a snow-debris-glacier column according to meteorological forcing and evolving thermal properties. It successfully produces variations in water content, phase, and location, demonstrating both diffusion and pooling at the glacier surface. And it computes glacier melt based on the processes of heat and water transfer, their determination of thermal and hydraulic properties, and their interplay with one another.

Improvement to the work presented in this study could be achieved through further constraints on the lateral runoff timescale (through, for example, laboratory or field-based experiments) and more detailed assimilation of the snow rate with the SR50 data. Snow is a strong insulator, and any error in simulated occurrence of snowfall will cause error in the surface temperatures and underlying debris temperature profile simulated by ISBA-DEB (e.g. Figure 6).

ISBA-DEB may be used to explore past or future changes in sub-debris melt. Reanalysis data, such as that of ERA Interim, provides all variables necessary to drive the model. Running ISBA-DEB under various Representative Concentration Pathway (RCP) emissions scenarios (Van Vuuren et al., 2011; Allen et al., 2014) would provide insight into the fate of ice under debris, an increasingly important topic as debris cover is increasing in a warming climate (Thakuri et al., 2014; Scherler et al., 2018).

https://doi.org/10.5194/tc-2019-168
Preprint. Discussion started: 10 September 2019

Code availability. <surfex_git2 @ V8_1_giese> code available at:
opensource.umr-cnrm.fr/projects/surfex_git2/repository?utf8=?&rev=V8_1_giese

Data availability. FORCING.nc and OPTIONS.nam files available at https://glacioclim.osug.fr/spip.php?article75&lang=fr

https://doi.org/10.5194/tc-2019-168
Preprint. Discussion started: 10 September 2019

The Cryosphere
Discussions

Model Parameter or Physical Constant	Value	Source/Note	Where specified
Ice density (kg m^{-3})	917		
Air density (kg m^{-3})	0.644-0.720		
Air thermal cond. (W m^{-1}K^{-1})	0.024	introduced in ISBA-DEB	
Air heat capacity (J kg^{-1}K^{-1})	1005	introduced in ISBA-DEB	
Water density (kg m^{-3})	1000		
Water thermal conductivity (W m^{-1}K^{-1})	0.57		
Water heat capacity (J kg^{-1}K^{-1})	4218		
Ice thermal conductivity (W m^{-1}K^{-1})	2.22		
Ice heat capacity (J kg^{-1}K^{-1})	2106		
Gravitational acceleration (m s^{-2})	9.80665		
Latent heat of vaporization of water (L_v) (J kg^{-1})	2.5008 $\times 10^6$		
Latent heat of sublimation of water (L_s) (J kg^{-1})	2.8345 $\times 10^6$		
Latent heat of fusion of water (L_m) (J kg^{-1})	3.337 $\times 10^5$		
Debris emissivity (ϵ)	0.94*	Reid and Brock (2010)	OPTIONS & modd_isba_par.F90
Debris albedo (α)	0.2*	calc. from SW measurements	OPTIONS
Dry debris density (kg m^{-3})	1690	measured	modd_isba_par.F90
Dry debris thermal cond. (W m^{-1}K^{-1})	0.94*	Reid and Brock (2010)	thrmcondz.F90
Dry debris heat capacity (J kg^{-1}K^{-1})	948	Reid and Brock (2010)	modd_isba_par.F90
Debris vol. heat cap. (J m^{-3}K^{-1})	1602120	-	-
Debris saturated hydraulic conductivity (k_{sat}, m s^{-1}), Layers 1-12	0.03	Domenico et al. (1998)	init_veg_pgdn.F90
Debris saturated hydraulic conductivity (k_{sat}, m s^{-1}), Layer 13	0		init_veg_pgdn.F90
Matric potential at saturation (Ψ_{sat}, m)	**		init_veg_pgdn.F90
b	**		init_veg_pgdn.F90
Debris porosity (Φ)	0.388465**, 0.999	$\sim$ 0.37 (measured)	init_veg_pgdn.F90
Debris surface z_{om} (m)	0.05*	Lejeune et al. (2013)	OPTIONS
Debris surface z_{om}/z_{oh} ratio (m)	10*	ISBA default, Mascart et al. (1995)	OPTIONS & ini_data_param.F90
Shape factor	30	tuned	hydro_soildif.F90
τ_{max} (s)	86400	tuned	hydro_soildif.F90
τ_{min} (s)	3600	Collier et al. (2014)	hydro_soildif.F90
Slope (^{o})	5*	measured	hydro_soildif.F90
$\alpha_{\wp}$	6	*	hydro_soildif.F90
w_{min} (m^{3}m^{-3})	0.0001	0.001 in ISBA	modd_isba_par.F90
Model time step (s)	900	with splitting in hydro_soildif.F90	OPTIONS
Number of calculation layers	13 debris, 7 ice	measured	OPTIONS
Debris layer thickness (cm)	12.5	measured	
Altitude of measurement site (m)	5360	measured	FORCING

Table A1. Physical constants as well as parameter values used in the baseline ISBA-DEB, before sensitivity tests performed on parameters with a single asterisk. Double asterisks appear in place of values predicted by pedotransfer functions (PTFs) of Noilhan et al. (1995) (using Clapp and Hornberger, 1978) based upon an input of 98% sand and 2% clay. The calculated porosity given by the PTFs is 0.39, close enough to the measured porosity of 0.37 (standard deviation = 0.04) that we did not overwrite the PTF calculation. The designation of zero hydraulic conductivity of the bottom debris layer simulates an impenetrable glacier surface and ensures no drainage out of the debris into the glacier. The third column of the table indicates the file in which these parameters are set, for the future user. Air density is a function, as described in the caption of Table 1.

https://doi.org/10.5194/tc-2019-168
Preprint. Discussion started: 10 September 2019

The Cryosphere Discussions

Author contributions. A. Giese conceived the study, performed the modeling work, and wrote the manuscript. A. Boone assisted in modeling work; he was instrumental in the coding of ISBA-DEB adaptations and in integrating them into ISBA. P. Wagnon made the meteorological forcing data and debris temperature data available for this study, and he provided invaluable feedback on the direction of the modeling work and on the specific model output. R. Hawley helped troubleshoot many modeling hurdles and advised on the methodology for the tuning and sensitivity tests.

Competing interests. There are no competing interests.

Acknowledgements. S. Morin provided an introduction and orientation to using SURFEX, and M. Lafaysse (Météo-France - Centre d'Etudes de la Neige, CEN) and S. Schwarz (Dartmouth) answered many technical questions. Y. Lejeune corrected precipitation data and together with M. Dumont facilitated A. Giese's work during a 10-month stay at CEN. G. Lewis provided valuable feedback and created the map. C. Vincent offered advising throughout the project, and Y. Arnaud helped define a direction and also gave feedback. We thank D. Shrestha, C. Vincent, Y. Arnaud, F. Brun, J. Shea and many other people who cannot be all listed for their assistance in the field. This work has been supported by the French Observatory CRYOBS-CLIM now part of the IR OZCAR, the French National Research Agency (ANR) through ANR-13-SENV-0005-04-PRESHINE, and by a grant from Labex OSUG@2020 (Investissements d'avenir - ANR10 LABX56). This study was carried out within the framework of the Ev-K2-CNR Project in collaboration with the Nepal Academy of Science and Technology as foreseen by the Memorandum of Understanding between Nepal and Italy. Thanks to contributions from the Italian National Research Council, the Italian Ministry of Education, University and Research and the Italian Ministry of Foreign Affairs. We thank Pyramid staff and Glacier Safari Treks for their logistical support. A. Giese was supported by NASA Space Grant NNX15AH79H and NSF GRF grant DGE-1313911.

https://doi.org/10.5194/tc-2019-168
Preprint. Discussion started: 10 September 2019

References

Allen, M. R., Barros, V. R., Broome, J., Cramer, W., Christ, R., Church, J. A., Clarke, L., Dahe, Q., Dasgupta, P., Dubash, N. K., et al.: IPCC fifth assessment synthesis report-climate change 2014 synthesis report, 2014.

Azam, M., Wagnon, P., Vincent, C., Ramanathan, A., Favier, V., Mandal, A., and Pottakkal, J.: Processes governing the mass balance of Chhota Shigri Glacier (western Himalaya, India) assessed by point-scale surface energy balance measurements, The Cryosphere, 8, 2195–2217, 2014.

Blum, W. E., Nortcliff, S., and Schad, P.: Essentials of soil science: soil formation, functions, use and classification (world reference base, WRB), Borntraeger, 2018.

Boone, A. and Etchevers, P.: An intercomparison of three snow schemes of varying complexity coupled to the same land surface model: Local-scale evaluation at an Alpine site, Journal of Hydrometeorology, 2, 374–394, 2001.

Boone, A., Calvet, J.-C., and Noilhan, J.: Inclusion of a third soil layer in a land surface scheme using the force–restore method, Journal of Applied Meteorology, 38, 1611–1630, 1999.

Boone, A., Masson, V., Meyers, T., and Noilhan, J.: The influence of the inclusion of soil freezing on simulations by a soil–vegetation–atmosphere transfer scheme, Journal of Applied Meteorology, 39, 1544–1569, 2000.

Brock, B. W., Mihalcea, C., Kirkbride, M. P., Diolaiuti, G., Cutler, M. E., and Smiraglia, C.: Meteorology and surface energy fluxes in the 2005–2007 ablation seasons at the Miage debris-covered glacier, Mont Blanc Massif, Italian Alps, Journal of geophysical research: atmospheres, 115, 2010.

Brooks, R. H. and Corey, A. T.: Properties of porous media affecting fluid flow, Journal of the Irrigation and Drainage Division, 92, 61–90, 1966.

Brun, F., Wagnon, P., Berthier, E., Shea, J. M., Immerzeel, W. W., Kraaijenbrink, P. D., Vincent, C., Reverchon, C., Shrestha, D., and Arnaud, Y.: Ice cliff contribution to the tongue-wide ablation of Changri Nup Glacier, Nepal, central Himalaya, The Cryosphere, 12, 3439–3457, 2018.

Clapp, R. B. and Hornberger, G. M.: Empirical equations for some soil hydraulic properties, Water resources research, 14, 601–604, 1978.

Collier, E., Nicholson, L., Brock, B., Maussion, F., Essery, R., and Bush, A.: Representing moisture fluxes and phase changes in glacier debris cover using a reservoir approach, The Cryosphere, 8, 1429–1444, 2014.

Collier, E., Nicholson, L., Brock, B., Maussion, F., Essery, R., and Bush, A.: Corrigendum to "Representing moisture fluxes and phase changes in glacier debris cover using a reservoir approach" published in The Cryosphere, 8, 1429–1444, 2014, The Cryosphere, 2016.

Conway, H. and Rasmussen, L.: Summer temperature profiles within supraglacial debris on Khunibu Glacier, Nepal, Debris covered glaciers, pp. 89–97, 2000.

Decharme, B., Boone, A., Delire, C., and Noilhan, J.: Local evaluation of the Interaction between Soil Biosphere Atmosphere soil multilayer diffusion scheme using four pedotransfer functions, Journal of Geophysical Research: Atmospheres, 116, 2011.

Decharme, B., Martin, E., and Faroux, S.: Reconciling soil thermal and hydrological lower boundary conditions in land surface models, Journal of Geophysical Research: Atmospheres, 118, 7819–7834, 2013.

Decharme, B., Brun, E., Boone, A., Delire, C., Le Moigne, P., and Morin, S.: Impacts of snow and organic soils parameterization on northern Eurasian soil temperature profiles simulated by the ISBA land surface model, The Cryosphere, 10, 853–877, 2016.

Domenico, P. A., Schwartz, F. W., et al.: Physical and chemical hydrogeology, vol. 506, Wiley New York, 1998.

https://doi.org/10.5194/tc-2019-168
Preprint. Discussion started: 10 September 2019

Evatt, G. W., Abrahams, I. D., Heil, M., Mayer, C., Kingslake, J., Mitchell, S. L., Fowler, A. C., and Clark, C. D.: Glacial melt under a porous debris layer, Journal of Glaciology, 61, 825–836, 2015.

Fujita, K. and Sakai, A.: Modelling runoff from a Himalayan debris-covered glacier, Hydrology and Earth System Sciences, 18, 2679–2694, 2014.

Fyffe, C., Reid, T., Brock, B., Kirkbride, M., Diolaiuti, G., Smiraglia, C., and Diotri, F.: A distributed energy-balance melt model of an alpine debris-covered glacier, Journal of Glaciology, 60, 587–602, 2014.

Giard, D. and Bazile, E.: Implementation of a new assimilation scheme for soil and surface variables in a global NWP model, Monthly weather review, 128, 997–1015, 2000.

Huintjes, E., Sauter, T., Schröter, B., Maussion, F., Yang, W., Kropáček, J., Buchroithner, M., Scherer, D., Kang, S., and Schneider, C.: Evaluation of a coupled snow and energy balance model for Zhadang glacier, Tibetan Plateau, using glaciological measurements and time-lapse photography, Arctic, antarctic, and alpine research, 47, 573–590, 2015.

Inoue, J. and Yoshida, M.: Ablation and heat exchange over the Khumbu Glacier, Journal of the Japanese Society of Snow and Ice, 41, 26–33, 1980.

Johnsson, H. and Lundin, L.-C.: Surface runoff and soil water percolation as affected by snow and soil frost, Journal of Hydrology, 122, 141–159, 1991.

Juen, M., Mayer, C., Lambrecht, A., Wirbel, A., and Kueppers, U.: Thermal properties of a supraglacial debris layer with respect to lithology and grain size, Geografiska Annaler: Series A, Physical Geography, 95, 197–209, 2013.

Kayastha, R. B., Takeuchi, Y., Nakawo, M., and Ageta, Y.: Practical prediction of ice melting beneath various thickness of debris cover on Khumbu Glacier, Nepal, using a positive degree-day factor, IAHS Publication, 7182, 2000.

Kowalewski, D. E., Marchant, D. R., Swanger, K. M., and Head III, J. W.: Modeling vapor diffusion within cold and dry supraglacial tills of Antarctica: Implications for the preservation of ancient ice, Geomorphology, 126, 159–173, 2011.

Kraaijenbrink, P., Bierkens, M., Lutz, A., and Immerzeel, W.: Impact of a global temperature rise of 1.5 degrees Celsius on Asia's glaciers, Nature, 549, 257, 2017.

Lejeune, Y., Bertrand, J.-M., Wagnon, P., and Morin, S.: A physically based model of the year-round surface energy and mass balance of debris-covered glaciers, Journal of Glaciology, 59, 327–344, 2013.

LeMoigne, P.: SURFEX Scientific Documentation, 2018.

Mascart, P., Noilhan, J., and Giordani, H.: A modified parameterization of flux-profile relationships in the surface layer using different roughness length values for heat and momentum, Boundary-Layer Meteorology, 72, 331–344, 1995.

Masson, V., Le Moigne, P., Martin, E., Faroux, S., Alias, A., Alkama, R., Belamari, S., Barbu, A., Boone, A., Bouyssel, F., et al.: The SURFEXv7. 2 land and ocean surface platform for coupled or offline simulation of earth surface variables and fluxes, 2013.

Miles, E. S., Steiner, J. F., and Brun, F.: Highly variable aerodynamic roughness length (z0) for a hummocky debris-covered glacier, Journal of Geophysical Research: Atmospheres, 122, 8447–8466, 2017.

Monin, A. and Obukhov, A.: Osnovnie haraktristiki turbulentnogo peremeshivaniya v prizemnom sloe atmosferi [Main characteristics of turbulent mixing in atmospheric boundary layer], Trudy Inst. Geofiz.(Akad. Nauk SSSR), 24, 163–187, 1954.

Nakawo, M. and Young, G. J.: Field experiments to determine the effect of a debris layer on ablation of glacier ice, Annals of Glaciology, 2, 85–91, 1981.

Nicholson, L. and Benn, D. I.: Calculating ice melt beneath a debris layer using meteorological data, Journal of Glaciology, 52, 463–470, 2006.

Nicholson, L. and Benn, D. I.: Properties of natural supraglacial debris in relation to modelling sub-debris ice ablation, Earth Surface Processes and Landforms, 38, 490–501, 2012.

Noilhan, J. and Mahfouf, J.-F.: The ISBA land surface parameterisation scheme, Global and planetary Change, 13, 145–159, 1996.

Noilhan, J. and Planton, S.: A simple parameterization of land surface processes for meteorological models, Monthly weather review, 117, 536–549, 1989.

Noilhan, J., , and Lacarrere, P.: GCM grid-scale evaporation from mesoscale modeling, Journal of climate, 8, 206–223, 1995.

Östrem, G.: Ice melting under a thin layer of moraine, and the existence of ice cores in moraine ridges, Geografiska Annaler, 41, 228–230, 1959.

Pritchard, H. D.: Asia's shrinking glaciers protect large populations from drought stress, Nature, 569, 649–654, 2019.

Quincey, D., Smith, M., Rounce, D., Ross, A., King, O., and Watson, C.: Evaluating morphological estimates of the aerodynamic roughness of debris covered glacier ice, Earth Surface Processes and Landforms, 42, 2541–2553, 2017.

Reid, T., Carenzo, M., Pellicciotti, F., and Brock, B.: Including debris cover effects in a distributed model of glacier ablation, Journal of Geophysical Research: Atmospheres, 117, 2012.

Reid, T. D. and Brock, B. W.: An energy-balance model for debris-covered glaciers including heat conduction through the debris layer, Journal of Glaciology, 56, 903–916, 2010.

Reijmer, C. H. and Hock, R.: Internal accumulation on Storglaciären, Sweden, in a multi-layer snow model coupled to a distributed energy- and mass-balance model, Journal of Glaciology, 54, 61–72, 2008.

Reznichenko, N., Davies, T., Shulmeister, J., and McSaveney, M.: Effects of debris on ice-surface melting rates: an experimental study, Journal of Glaciology, 56, 384–394, 2010.

Rounce, D. and McKinney, D.: Debris thickness of glaciers in the Everest area (Nepal Himalaya) derived from satellite imagery using a nonlinear energy balance model, The Cryosphere, 2014.

Rounce, D., Quincey, D., and McKinney, D.: Debris-covered glacier energy balance model for Imja–Lhotse Shar Glacier in the Everest region of Nepal, The Cryosphere, 9, 2295–2310, 2015.

Sakai, A., Fujita, K., and Kubota, J.: Evaporation and percolation effect on melting at debris-covered Lirung Glacier, Nepal Himalayas, 1996, Bulletin of glaciological research, 21, 9–16, 2004.

Scherler, D., Wulf, H., and Gorelick, N.: Global Assessment of Supraglacial Debris-Cover Extents, Geophysical Research Letters, 45, 11–798, 2018.

Sherpa, S. F., Wagnon, P., Brun, F., Berthier, E., Vincent, C., Lejeune, Y., Arnaud, Y., Kayastha, R. B., and Sinisalo, A.: Contrasted surface mass balances of debris-free glaciers observed between the southern and the inner parts of the Everest region (2007–15), Journal of Glaciology, 63, 637–651, 2017.

Smeets, C. and Van den Broeke, M.: The parameterisation of scalar transfer over rough ice, Boundary-layer meteorology, 128, 339, 2008.

Steiner, J. F., Litt, M. H., Stigter, E. E., Shea, J. M., Bierkens, M. F., and Immerzeel, W. W.: The Importance of Turbulent Fluxes in the Surface Energy Balance of a Debris-Covered Glacier in the Himalayas, Frontiers in Earth Science, Cryosphere, 6, 2018.

Takeuchi, Y., Kayastha, R. B., and Nakawo, M.: Characteristics of ablation and heat balance in debris-free and debris-covered areas on Khumbu Glacier, Nepal Himalayas, in the pre-monsoon season, IAHS PUBLICATION, pp. 53–62, 2000.

Thakuri, S., Salerno, F., Smiraglia, C., Bolch, T., D'Agata, C., Viviano, G., and Tartari, G.: Tracing glacier changes since the 1960s on the south slope of Mt. Everest (central Southern Himalaya) using optical satellite imagery, Global and Planetary Change, 8, 1297–1315, 2014.

https://doi.org/10.5194/tc-2019-168
Preprint. Discussion started: 10 September 2019

Van Vuuren, D. P., Edmonds, J., Kainuma, M., Riahi, K., Thomson, A., Hibbard, K., Hurtt, G. C., Kram, T., Krey, V., Lamarque, J.-F., et al.: The representative concentration pathways: an overview, Climatic change, 109, 5, 2011.

Vincent, C., Wagnon, P., Shea, J., Immerzeel, W., Kraaijenbrink, P., Shrestha, D., Soruco, A., Arnaud, Y., Brun, F., Berthier, E., et al.: Reduced melt on debris-covered glaciers: investigations from Changri Nup Glacier, Nepal, The Cryosphere, 10, 1845–1858, 2016.

Wagnon, P., Lafaysse, M., Lejeune, Y., Maisincho, L., Rojas, M., and Chazarin, J.-P.: Understanding and modeling the physical processes that govern the melting of snow cover in a tropical mountain environment in Ecuador, Journal of Geophysical Research: Atmospheres, 114, 2009.

Zuo, Z. and Oerlemans, J.: Modelling albedo and specific balance of the Greenland ice sheet: calculations for the Søndre Strømfjord transect, Journal of Glaciology, 42, 305–317, 1996.